Integrating network pharmacology and experimental studies for uncovering the molecular mechanisms of *Dioscorea bulbifera* L. in the treatment of thyroid cancer

Ziqi Liu [a,1], Lian Zhong [a,1], Lingyu Wang [a], Meiyan Li [a], Chao Chen [b,*]

[a] School of Pharmacy, Chengdu University of Traditional Chinese Medicine, Chengdu, 611137, PR China
[b] Sichuan Provincial People's Hospital, School of Medicine, University of Electronic Scienceand Technology of China, Chengdu 610072, P.R. China

A B S T R A C T

Introduction: Thyroid cancer (TC), a common endocrine malignant tumor with a higher incidence in females than in males, is a serious threat to human life and health. Although current clinical treatments can alleviate this disease, the recurrence rate remains high. Tuber *Dioscoreae Bulbiferae*, also called *Huang-Yao-Zi* (HYZ), has remarkable curative properties, few side effects and is used for the treatment of sore throat, goiter, hemoptysis, and other diseases in traditional Chinese medicine (TCM). Existing clinical studies have found that HYZ can improve the clinical symptoms of TC patients and reduce tumor volume, while in vitro studies have found that HYZ can induce the death of thyroid cancer cells. However, the mechanism of HYZ in the treatment of TC is still unclear.
Methods: In this study, based on network pharmacology and bioinformatics, the target and molecular mechanism of HYZ in the treatment of TC were preliminarily explored. The results suggest that the antithyroid cancer effect of HYZ may be related to the PI3K-Akt and focal adhesion pathways. Then, a TC cell model was established to further explore the detail molecular mechanisms.
Results: Fortunately, HYZ induced apoptosis in KMH-2 cells and regulated the expression of apoptosis-related proteins and genes. At the same time, HYZ can also significantly inhibit the migration and invasion of TC cells. Further studies showed that the pharmacological activities of HYZ were related to the regulation of the PI3K-Akt and focal adhesion pathways.
Conclusion: Our study provides a reference for further animal or clinical studies investigating the effectiveness and molecular mechanisms of HYZ against thyroid cancer.

1. Introduction

At present, cancer is a very prominent public health problem worldwide, seriously threatening human life and health. In China, lung cancer, thyroid cancer (TC), stomach cancer and other malignant tumors account for more than 75% of all new cases [1–3]. TC is one of the most common endocrine malignant tumors, and the incidence rate continues to increase every year [4]. In addition, TC is three times more common in women than in men. The pathogenesis of thyroid cancer is still unclear, but iodine intake, genetic factors,

---

radiation exposure, and other factors, such as sex hormones, are thought to be the main causes of thyroid cancer [5]. TC often presents as a painless neck mass or nodule, and the tumor can compress the esophagus and trachea [6]. At present, the clinical treatment for TC is mainly surgical resection combined with postoperative drugs and local radiotherapy. Although the curative effect is good, the subsequent recurrence rate is still very high, and the adverse reactions brought by the treatment seriously increase the pain suffered by patients. In addition, the high cost of treatment increases the financial burden of patients [7]. Therefore, it is necessary to develop low-cost, effective, and safe complementary or alternative antithyroid cancer drugs.

Tuber *Dioscoreae Bulbiferae* (*Huang-Yao-zi*, HYZ), is the dried tuber of *Dioscorea Bulbifera* L., also known as *Hong Yaozi*, *Ku Yaozi*, *Huang Gouzi*, and so on. This medication has the effect of clearing heat, detoxifying, cooling blood and detumescence and is used for the treatment of sore throat, goiter, vomiting blood, hemoptysis and so on [8,9]. In recent years, with the deepening of research, scholars have found that the chemical composition of HYZ is complex, including astragalus, flavonoids, diterpenoid lactones and other components, with anti-inflammatory, antitumor, antiviral, and other pharmacological activities [10–17]. Modern clinical application also found that HYZ and its prescription can significantly improve the symptoms of thyroid tumor and TC patients and reduce the size of tumor tissue [18–21]. Modern studies have also shown that HYZ can inhibit the growth of human TC cells by downregulating the mRNA and protein expression of SW579 Surviving [22]. However, the molecular mechanism of HYZ against TC is still unclear. Therefore, in this study, we used network pharmacology combined experimental studies to study the therapeutic effect of HYZ on TC and explore its molecular mechanism.

2. Materials and methods

Ethical statement

All experimental protocols were strictly followed in accordance with the International Ethical Guidelines for Biomedical Research Involving Human Subjects, and all the experimental protocols were carried out with the approval of the Ethics Committee of the Chengdu University of Traditional Chinese Medicine (No. 2019-08).

3. Reagents and materials

Trans Serum EQ Fetal Bovine Serum (FBS) was purchased from TransGen Biotech (Beijing, China), and the prestained protein marker was obtained from Accurate Biotechnology (Hunan) Co., Ltd. (Hunan, China); RAPI buffer, nuclear protein extraction kit, BCA protein assay reagent, primary antibodies for c-Caspase 3, phosphorylation- (p-)-Bad, Bad and β-actin were purchased from the Boster Biological Technology Company (Wuhan, China); Annexin V-FITC/PI kit was purchased from Multisciences (Lianke) Biotechnology Corporate Limited (Hangzhou, China); CCK-8 kits were obtained from US Everbright Inc. (Suzhou, China); enhanced chemiluminescence (ECL) luminescence reagent and a cell cycle detection kit were purchased from Beijing 4A Biotech Co. (Beijing, China); primary antibodies for FAK, p-FAK, and E-CAD were purchased from Cell Signaling Technology Co. (Danvers, MA, USA); and protein kinase B (Akt), p-Akt, phosphoinositide 3-kinase (PI3K), p-PI3K and goat-anti-rabbit/rat horseradish peroxidase-conjugated (HRP) secondary antibodies were purchased from Abcam (Cambridge, MA, USA).

4. Component retrieval of HYZ

The key words "*Tuber Dioscoreae Bulbiferae*" were searched in the TCMSP database to collect the chemical components of HYZ [23]. Meanwhile, the compound library of HYZ was supplemented by literature mining. Oral bioavailability (OB) is one of the most important parameters in pharmacokinetic evaluation of drug absorption distribution, metabolism, and excretion, reflecting the speed and degree of absorption of the active ingredients in oral drugs into the body circulation, and is also an important indicator to evaluate whether oral drugs can exert efficacy. The Dl-like property (DL) value represents the similarity between the ingredients and the known chemical drugs, which has important reference value for determining whether the ingredients of traditional Chinese medicine (TCM) exert effects in the body [24]. Considering the medicinal properties of the active ingredients in HYZ, we selected compounds with OB $\geq$ 30% and DL $\geq$ 0.18 as the 24 potential active ingredients of HYZ.

5. Target collection of HYZ

The targets of the active components of HYZ were collected from the TCMSP database and supplemented with literature mining. In addition, the active components of HYZ were uploaded to PharmMapper (http://www.lilab-ecust.cn/pharmmapper/) [25–27] and Swiss Target Prediction (http://www.swisstargetprediction.ch/) [28,29], and the action targets of these components were obtained through reverse docking. Finally, the results of TCMSP, PharmMapper and Swiss Target Prediction were combined to delete repeated targets and construct component-target data pairs. The UniProt (https://www.uniprot.org/) database was used to correct the gene standard names of the obtained targets and finally obtain the target library of the active components of HYZ.

6. Collection of TC targets

The GEO database is an open public database that stores the experimental results of high-throughput sequencing of various microarray chips. With "thyroid cancer" as the key word, all data sites that study gene expression differences in thyroid tissues of

cancer patients and normal people were searched in the GEO database. Finally, the gene expression profile dataset GSE3678 was collected, which included 7 papillary TC tissue samples and 7 normal thyroid tissue samples. Background correction and data normalization were performed on the dataset with the help of the GEO2R online tool, and the genes with an FDR value < 0.05, | Log2FC| > 1 were screened as differentially expressed genes (DEGs). Finally, the target library of TC was obtained, and the volcano map of GSE3678 was analyzed and visualized by using the online SangerBox tool (http://www.sangerbox.com/).

6.1. Protein–protein interaction network (PPI)

The intersection of the HYZ target library and TC target library was processed, and the overlapping target was used as the possible target for HYZ to improve TC. The obtained overlapping genes were uploaded to the string database (https://string-db.org/), and the species was restricted to humans to obtain the data pairs of interactions between these targets. The data pairs were imported into Cytoscape software to construct a protein–protein interaction network (PPI), in which nodes represented targets and edges represented interaction relationships between targets. The network structure of PPI was analyzed by the network analyzer plug-in, and the hub gene in PPI was screened out.

6.2. Drug-component-target-disease network diagram (DCTD)

The drug-component, component-target and target-disease data pairs were constructed using R language software and then imported into Cytoscape software to construct a drug-component-target-disease network diagram (DCTD). In the network diagram, nodes represent potential active ingredients and targets, and edges represent the corresponding relationship between ingredients and targets. Network structure was analyzed through the network analyzer plug-in, and network topology parameters such as degree were calculated to analyze the main active components and action targets of HYZ in improving TC and to further scientifically and reasonably clarify the material basis and action mechanism of HYZ in improving TC.

6.3. Kyoto Encyclopedia of Genes and Genomes (KEGG) and Gene Ontology (GO) analysis

Gene Ontology (GO) functional annotation and Kyoto Encyclopedia of Genes and Genomes (KEGG) pathway enrichment analysis of overlapping genes were performed using the cluster Profiler toolkit of R language software. In the analysis, species were set as human sources, enrichment results with P < 0.05 were defined as having significant significance, and a relevant bar chart bubble chart was drawn.

7. Preparation of lyophilized powder from HYZ

HYZ was purchased from Neautus Chinese Herbal Pieces Ltd. Co. (Chengdu, China) and identified as the whole grass of *Dioscorea Bulbifera* L. by Prof. Chunjie Wu (School of Pharmacy, Chengdu University of TCM). The samples of HYZ were kept in the library (No. HYZ-01). We took an appropriate amount of HYZ, added eight times the amount of distilled water to soak for 1 h, boiled it on high heat, then boiled it on low heat for 1 h. Then, we filtered the residue to take the filtrate, filtered the filtrate with filter paper, and freeze dried the filtrate with a lyophilizer to obtain the lyophilized powder of HYZ water extract, which was stored in the refrigerator at −20 °C for reserve.

7.1. Cell culture

KMH-2 cells were purchased from Beina Biological Co. (Beijing, China) and cultured in DMEM containing 10% FBS and 1% penicillin at 37 °C in a humidified 5% CO2 atmosphere. The new medium was replaced every 2 days, and the cells were subcultured every 3 days. Three to five generations of cells were selected for the experiments in this study.

7.2. Cell viability detection

The CCK8 kit was used to determine the effect of HYZ on cell viability. KMH-2 cells at the logarithmic growth stage were prepared into a single-cell suspension and then inoculated into 96-well plates at 1×10^4 cells/well. They were placed in a 37 °C constant temperature incubator for 12 h, and then different concentrations of HYZ (0–120 μg/mL) were added for 24 h, 48 h and 72 h. At the end of the experiment, 10 μL CCK-8 solution was added to each well and incubated for half an hour at 37 °C. The OD value of each well was determined at 490 nm using a microplate reader, and cell viability was calculated using the following formula.

$$\text{Cell survival rate } (\%) = \left(\text{OD}_{\text{Drug}} - \text{OD}_{\text{Blank}}\right) / \left(\text{OD}_{\text{Normal}} - \text{OD}_{\text{Blank}}\right) \times 100\%$$
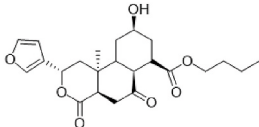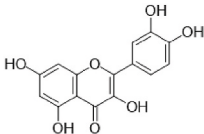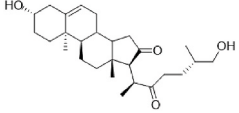
Wound Healing The effect of HYZ on KMH-2 cell migration was determined by a wound healing test. KMH-2 cells (1×10^6) were inoculated into 6-well plates and cultured in DMEM complete medium containing 10% PBS for 24 h. When the cells were fused to 90%, serum-free medium was replaced for 12 h. Then, a 200 μL spear was used to make cross wounds at the bottom of the orifice plate, and the experiment was incubated with different concentrations of HYZ (10, 20, 40 μg/mL) for 0 h, 6 h, 12 h and 24 h. At the end of the experiment, scratch images were collected under a microscope at each time period, and the scratch area was measured and analyzed

Table 1

Potential active compounds in *Dioscorea bulbifera*.

ID	Mol ID	Name	MW	OB	MF	DL	Structure
C1	MOL000239	Jaranol	314.31	50.83	$C_{17}H_{14}O_6$	0.29	
C2	MOL000358	beta-sitosterol	414.79	36.91	$C_{30}H_{52}O$	0.75	
C3	MOL000422	Kaempferol	286.25	41.88	$C_{15}H_{10}O_6$	0.24	
C4	MOL000449	Stigmasterol	412.77	43.83	$C_{29}H_{48}O$	0.76	
C5	MOL000546	Diosgenin	414.69	80.88	$C_{27}H_{42}O_3$	0.81	
C6	MOL000073	ent-Epicatechin	290.29	48.96	$C_{15}H_{14}O_6$	0.24	
C7	MOL007939	Diosbulbin B	344.39	43.01	$C_{19}H_{20}O_6$	0.7	
C8	MOL000096	(−)-Catechin	290.29	49.68	$C_{15}H_{14}O_6$	0.24	
C9	MOL009772	3,5,3′-trimethoxyquercetin	374.37	37.83	$C_{18}H_{16}O_7$	0.44	
C10	MOL009783	Diosbuibin I	506.59	37.93	$C_{29}H_{30}O_8$	0.86	
C11	MOL009788	Diosbulbin A	376.44	39.52	$C_{20}H_{24}O_7$	0.65	
C12	MOL009789	Diosbulbin C	362.41	65.87	$C_{19}H_{22}O_7$	0.6	

(*continued on next page*)

Table 1 (*continued*)

ID	Mol ID	Name	MW	OB	MF	DL	Structure
C13	MOL009794	Diosbulbin H	418.53	55.62	$C_{23}H_{30}O_7$	0.7	
C14	MOL000098	Quercetin	302.25	46.43	$C_{15}H_{10}O_7$	0.28	
C15	MOL009800	Kryptogenin	430.69	35.11	$C_{27}H_{42}O_4$	0.81	

MW, Molecular weight; MF, Molecular formula.

using ImageJ software.

7.2.1. Cell migration assay

The effect of HYZ on KMH-2 cell migration was determined by a transwell chamber. In brief, KMH-2 cells (1×10^5) were resuspended in FBS-free DMEM and inoculated in the upper chamber of a Transwell chamber. The lower chamber of the transwell chamber was filled with DMEM containing 20% FBS. Meanwhile, the cells were treated with different concentrations of HYZ (10, 20, 40 μg/mL) for 24 h. At the end of the experiment, the cells were placed into crystal violet staining solution for staining, and then cotton swabs were used to gently remove the cells in the inner side of the upper ventricle membrane. The cells on the outer side of the membrane were considered to be successfully migrated cells, and migration images were collected under the microscope.

7.2.2. Cell invasion assay

Transwell chambers were used to determine the effect of HYZ (10, 20, 40 μg/mL) on the invasion ability of KMH-2 cells. At 37 °C, the Transwell membrane was pretreated with 0.1% Matrigel for 30 min and then washed with PBS 3 times. The procedure was similar to that of the transwell migration experiment. Cell invasion was observed under a light microscope.

8. Apoptosis was detected by flow cytometry

The Annexin V-FITC/PI apoptosis assay kit was used to determine the effect of HYZ (20, 40, 60 μg/mL) on apoptosis of KMH-2 cells. In simple terms, cells in logarithmic growth phase were inoculated into 6-well plates with 1×10^6/wells and incubated in a 37 °C constant temperature incubator for 12 h, followed by intervention with different concentrations of HYZ for 24 h. At the end of the experiment, cells were collected, washed with precooled PBS twice, and the supernatant was centrifuged. The cells were suspended in 500 μL binding buffer, mixed with 5 μL Annexin V-FITC and 5 μL PI, and incubated at room temperature for 15 min. The apoptosis rate of the cells was determined by flow cytometry (BD, New York, NY, USA).

8.1. Western blot (WB)

Western blot (WB) assays were used to detect the effect of HYZ (20, 40, 60 μg/mL) intervention on protein expression in cells. In simple terms, cells in the logarithmic growth phase were inoculated into 6-well plates at 1×10^5 cells/well and incubated in a 37 °C constant temperature incubator for 12 h, followed by 24 h of treatment with different concentrations of HYZ. At the end of the experiment, RIPA cell lysis solution was used to extract total cell protein, and a BCA kit was used to detect the cell protein concentration. Then, an appropriate amount of 5 × protein loading buffer was added, and the protein was blown and mixed and boiled in 90 °C water baths for 10 min to desaturate the protein. Finally, sodium dodecyl sulfate−polyacrylamide gel electrophoresis (SDS−PAGE) was used to isolate total cell proteins and transfer them to PVDF membranes, which were placed in a blocking solution at room temperature for 1 h and then washed with TBST three times. The membrane and the corresponding primary antibody (Bad, p-Bad, PI3K, p-PI3K, Akt, p-Akt, FAK, p-FAK, E-CAD, β-actin) were incubated overnight at 4 °C and then incubated with HRP-labeled secondary antibody at room temperature for 1 h. Finally, the PVDF membrane was developed with ECL sensitizer, and the protein band images were photographed and saved.

8.2. Analysis and statistics

The mean and standard deviation (SD) were used for statistical analysis. SPSS 18.0 software was used for statistical analysis. 0.05 was considered statistically significant. All experiments were repeated three times.

9. Results

9.1. HYZ compound library and target library

Through database and literature retrieval, the OB and DL values of the compounds were limited, and a total of 15 potential active ingredients were obtained. Information on these compounds is shown in Table 1. The targets of these 15 potential active compounds were obtained by reverse docking in the PharmMapper and SwissTargetPrediction online databases, and the repeated targets were removed. Finally, a total of 640 targets were obtained, which is the target database of 15 potential active compounds in HYZ.

9.2. Target library for TC

The gene expression of "GSE3678" was analyzed, and the DEGs between thyroid tissues of TC patients and normal thyroid tissues were deleted and selected. Finally, 668 DEGs were obtained, among which 402 genes were upregulated and 266 were downregulated (Fig. 1A). Finally, 50 overlapping genes were obtained by comparing these DEGs with predicted targets of potential active components of HYZ (Fig. 1B).

9.3. PPI of HYZ against TC

The interaction between overlapping genes was analyzed with the help of the String online database and Cytoscape software, and the PPI network graph was constructed. As shown in Fig. 2A, there were 38 nodes in the network and 97 interaction relationships. Through the analysis of hub genes in the network, it was found that FN1 JUN AR RUNX2 FOS BMP2 MET and other targets had a large degree, suggesting that these genes were important targets for HYZ to play anti-TC roles (Fig. 2B).

9.4. Analysis of the DCTD

Cytoscape software was used to construct a DCTD, as shown in Fig. 2C. There were 63 nodes in the network diagram, including 15 compounds and 48 protein targets. In addition, the network has 194 edges, and there is not a single correspondence between the target and compound. One target corresponds to multiple compounds, and one compound can act on multiple targets, suggesting that HYZ can play an anti-TC role by acting on multiple targets through multiple components. Further analysis of the structure and topological parameters of the network diagram showed that C1, C14, C11, C3, C6, C8, C5, C9 and other compounds had the most targets, suggesting that these compounds played a core role in the network diagram, indicating that these compounds were the main active components of HYZ against TC (Table 2).

9.5. GO function and KEGG signal pathway enrichment analysis

R language software was used for GO function enrichment analysis of overlapping genes, and the analysis results are shown in Fig. 3A and B and Table 3. These overlapping genes were enriched in 591 GO functions, among which 520 were biological processes (BP), mainly including cellular response to oxidative stress; cellular response to chemical stress; hormone metabolic process; response to reactive oxygen species; cellular response to reactive oxygen species; response to oxidative stress; olefinic compound metabolic process; cyclic nucleotide catabolic process; cellular hormone metabolic process; and C21-steroid hormone metabolic process. In addition, 12 cellular components (CC) were accumulated, including platelet alpha granule lumen; basal part of cell, invadopodium;
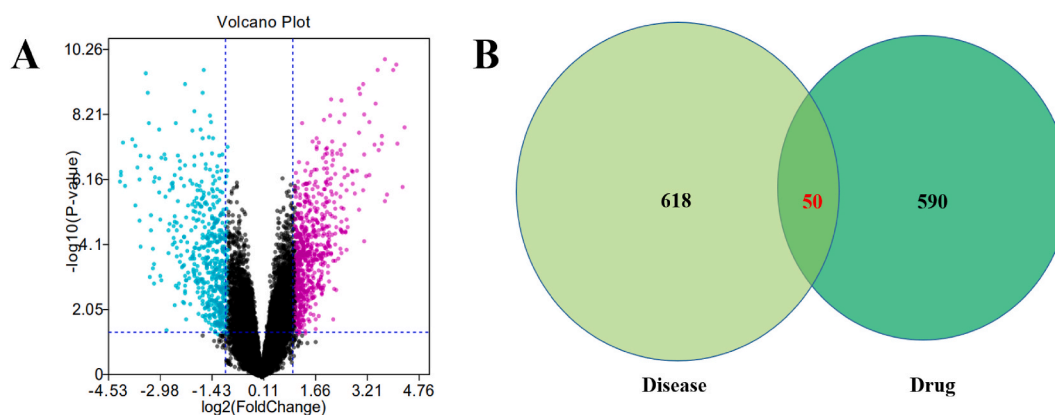
Fig. 1. Differently expressed genes screening. (**A**) The volcano plot of the differently expressed genes. (**B**) Overlapping genes of thyroid cancer (TC) and HYZ. Bottle green circle is the predictive gene in HYZ (590), the aqua circle is the DEGs in thyroid tissue of thyroid Cancer patients and normal patients (618), and the overlap in the middle is the overlapping genes between the two genes (50).
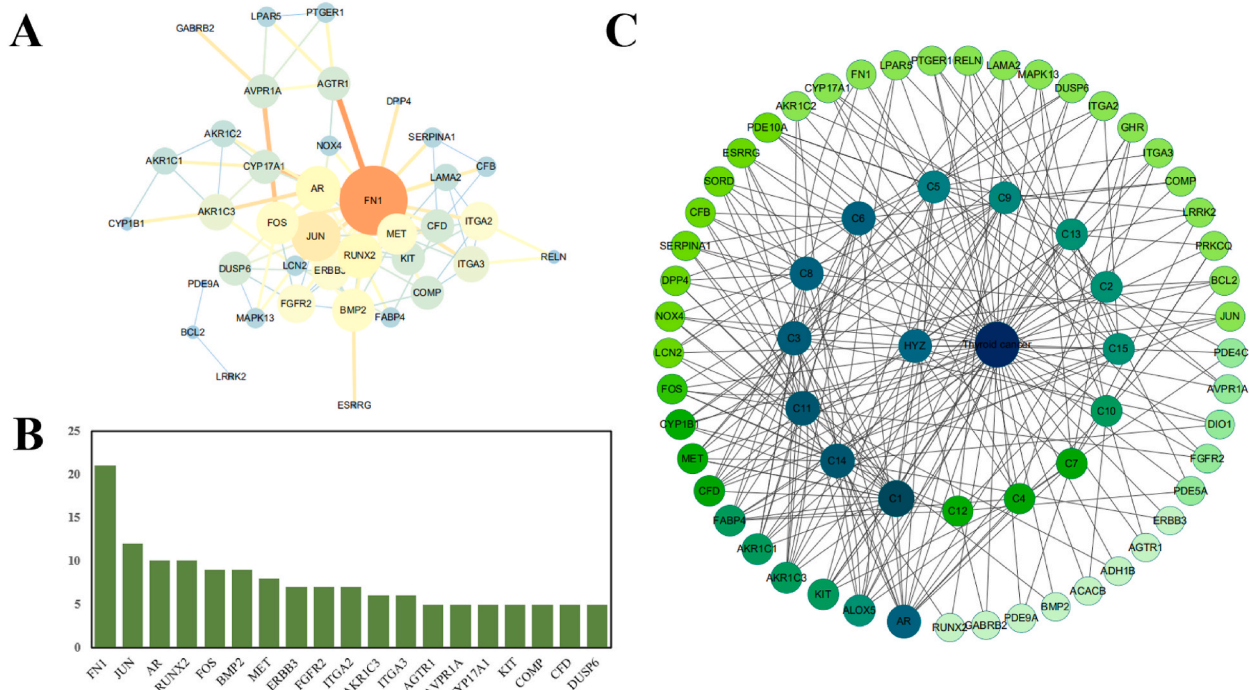
Fig. 2. Network analysis. (**A**) The PPI network of overlapping genes. (**B**) The 19 hub genes of higher interplay. (**C**) Network diagram of drug-component-target-disease network diagram (DCTD).

Table 2
Topological parameters of compound components in the drug-component-target-disease network diagram (Top 15).

Name	Degree	Average Shortest PathLength	Betweenness Centrality	Closeness Centrality	Neighborhood Connectivity
C1	24	2.140625	0.049463	0.467153	6.75
C14	18	2.265625	0.036134	0.441379	6.125
C11	18	2.203125	0.041581	0.453901	6.222222
C3	17	2.328125	0.026258	0.42953	6.642857
C6	16	2.296875	0.023127	0.435374	6.866667
C8	16	2.296875	0.022408	0.435374	6.866667
C5	12	2.390625	0.021567	0.418301	6.666667
C9	11	2.421875	0.013639	0.412903	7.272727
C2	10	2.453125	0.015284	0.407643	6.4
C13	10	2.484375	0.011212	0.402516	6.333333
C15	10	2.453125	0.013949	0.407643	7.5
C10	9	2.484375	0.014063	0.402516	6
C4	8	2.515625	0.008813	0.397516	7.375
C7	8	2.515625	0.010184	0.397516	6.875
C12	7	2.546875	0.008027	0.392638	6.428571

secretory granule lumen; and cytoplasmic vesicle lumen. There were 59 molecular functions (MFS), mainly including protease binding; 3′,5′-cyclic-nucleotide phosphodiesterase activity; cyclic-nucleotide phosphodiesterase activity; oxidoreductase activity, acting on the CH–OH group of donors, NAD or NADP as acceptors; oxidoreductase activity, acting on the CH–OH group of donors; monocarboxylic acid binding; bile acid binding; alditol: NADP+ 1-oxidoreductase activity; 3′,5′-cyclic-GMP phosphodiesterase activity; and mono-oxygenase activity. These results suggest that HYZ plays an important role in TC by regulating the oxidative stress response and metabolism. The histogram (Fig. 3A) and bubble diagram (Fig. 3B) of GO enrichment are shown in Fig. 3.

The KEGG pathway enrichment analysis of overlapping genes revealed that these genes were enriched in 19 obvious pathways, mainly including the PI3K-Akt signaling pathway, focal adhesion, ECM-receptor interaction, AGE-RAGE signaling pathway in diabetic complications, steroid hormone biosynthesis, small cell lung cancer, ovarian steroidogenesis, MAPK signaling pathway, EGFR tyrosine kinase inhibitor resistance, PD-L1 expression and PD-1 checkpoint pathway in cancer. These results indicate that active components in HYZ may synergically play an anti-TC role in multiple signaling pathways. The histogram (Fig. 4A) and bubble diagram (Fig. 4B) of KEGG enrichment are shown in Fig. 4.
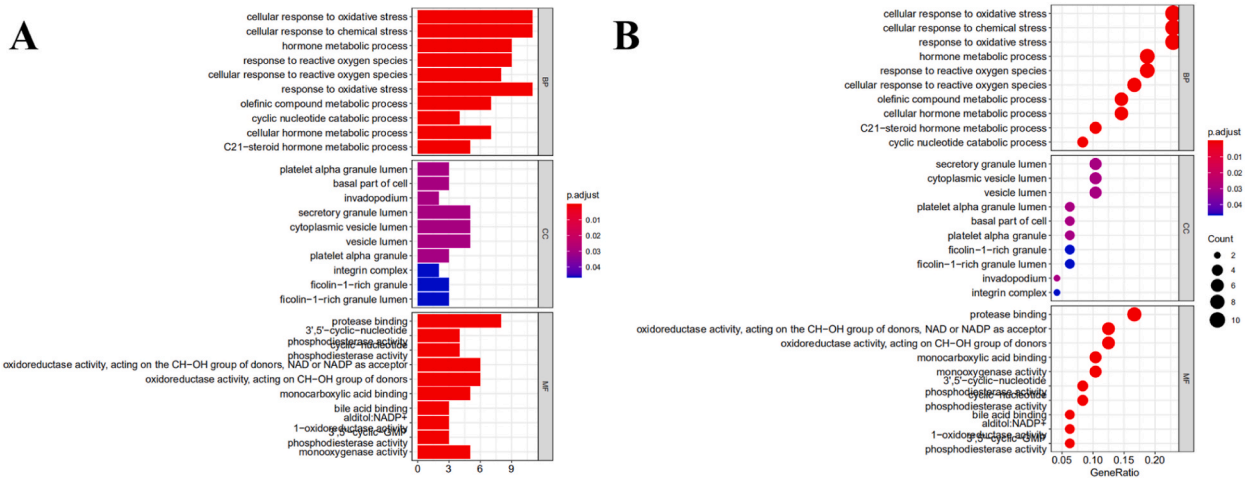
Fig. 3. GO enrichment. (**A**) GO functional enrichment analysis represented in bar chart. (**B**) GO functional enrichment analysis represented in bubble diagram.

Table 3
KEGG pathway enrichment analysis.

ID	Description	Gene Ratio	Bg Ratio	P value	p. adjust	Q value
hsa04151	PI3K-Akt signaling pathway	13/47	354/8108	6.15E-08	1.08E-05	7.38E-06
hsa04510	Focal adhesion	9/47	201/8108	1.78E-06	0.000156783	0.000106897
hsa04512	ECM-receptor interaction	6/47	88/8108	1.03E-05	0.000606736	0.000413683
hsa04933	AGE-RAGE signaling pathway in diabetic complications	6/47	100/8108	2.16E-05	0.000864446	0.000589395
hsa00140	Steroid hormone biosynthesis	5/47	61/8108	2.46E-05	0.000864446	0.000589395
hsa05222	Small cell lung cancer	5/47	92/8108	0.000177551	0.005101481	0.003478283
hsa04913	Ovarian steroidogenesis	4/47	51/8108	0.000202900	0.005101481	0.003478283
hsa04010	MAPK signaling pathway	8/47	294/8108	0.000248934	0.005476545	0.003734008
hsa01521	EGFR tyrosine kinase inhibitor resistance	4/47	79/8108	0.001083577	0.021189959	0.014447699
hsa05235	PD-L1 expression and PD-1 checkpoint pathway in cancer	4/47	89/8108	0.001688007	0.028011339	0.019098640
hsa04658	Th1 and Th2 cell differentiation	4/47	92/8108	0.001907410	0.028011339	0.019098640
hsa04657	IL-17 signaling pathway	4/47	94/8108	0.002064218	0.028011339	0.019098640
hsa05171	Coronavirus disease - COVID-19	6/47	232/8108	0.002069019	0.028011339	0.019098640
hsa01522	Endocrine resistance	4/47	98/8108	0.002404233	0.028797784	0.019634852
hsa04020	Calcium signaling pathway	6/47	240/8108	0.002454357	0.028797784	0.019634852
hsa04660	T cell receptor signaling pathway	4/47	104/8108	0.002983900	0.032333384	0.022045489
hsa04928	Parathyroid hormone synthesis, secretion and action	4/47	106/8108	0.003196652	0.032333384	0.022045489
hsa04659	Th17 cell differentiation	4/47	107/8108	0.003306823	0.032333384	0.022045489
hsa05145	Toxoplasmosis	4/47	112/8108	0.003896789	0.036096573	0.024611300
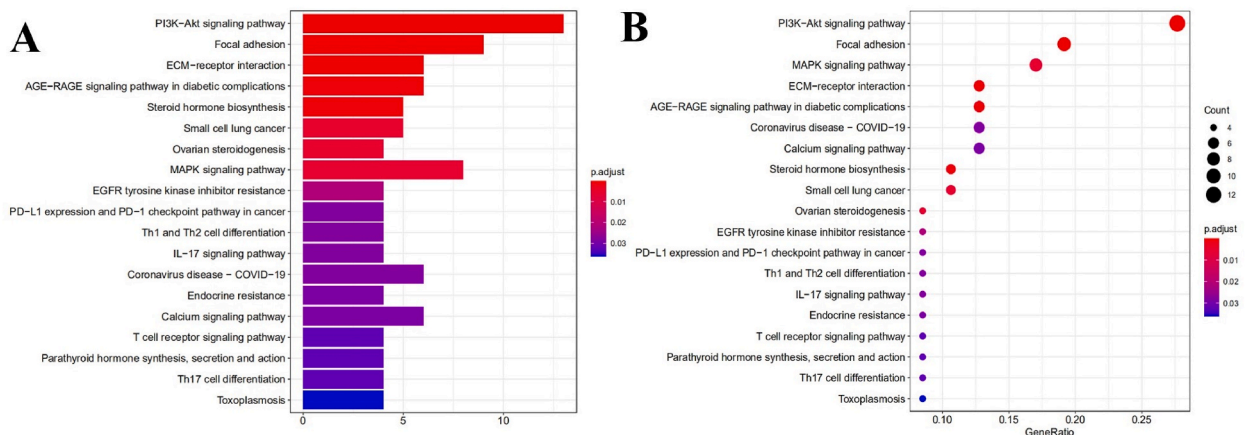
Fig. 4. KEGG enrichment. (**A**) Histogram of KEGG enrichment results; (**B**) Bubble diagram of KEGG enrichment results.

9.6. HYZ inhibits the viability of TC cells

The preliminary results of network pharmacology suggested that the antithyroid cancer effect of HYZ was related to the PI3K-Akt and focal adhesion pathways. Therefore, we established an in vitro model of TC cells (KMH-2 cells) to further study the effect of HYZ on TC cells in vitro and explore the possible mechanism. As shown in Fig. 5 A-C, the cell viability of KMH-2 cells was significantly inhibited after the addition of HYZ within 72 h, and the inhibition showed a significant time- and dose-dependent relationship. In subsequent experiments, we selected concentrations of 20 μg/mL, 40 μg/mL, and 80 μg/mL for 24 h as the method of HYZ administration.

9.7. HYZ inhibits the migration of TC cells

As shown in Fig. 6 A & 6B, with increasing time, the scratches of each group of cells gradually healed. At 24 h, the scratches prepared by pipetting gun tips in the control group almost healed completely, but the cell scars in the positive group and the HYZ group did not heal completely, suggesting that HYZ can significantly inhibit the scratch healing ability of KMH-2 cells, and this inhibition showed a significant time and dose dependence. Similarly, Transwell assays revealed a significant reduction in the number of cells migrating in the positive and HYZ groups compared with the control group (Fig. 7A). These results suggest that HYZ may inhibit the migration of KMH-2 cells.

9.8. HYZ inhibits the invasion of TC cells

In addition, the effect of HYZ on the invasion ability of KMH-2 cells was determined by transwell assay. As shown in Fig. 7B, compared with the control group, the number of invaded cells was significantly reduced in both the positive and HYZ groups at the end of the intervention, indicating that HYZ has a similar effect to the positive drug and can inhibit the invasion of TC cells.

9.9. HYZ can induce apoptosis of KMH-2 cells

To further explore the specific mechanism of the effect of HYZ on KMH 2 cell viability, flow cytometry was used to determine whether the antitumor effect of HYZ was related to apoptosis. As shown in Fig. 8 A-E, the apoptosis rate was significantly increased after HYZ intervention compared with the control group. These results indicated that the effect of HYZ on KMH-2 cell viability was related to the induction of apoptosis.
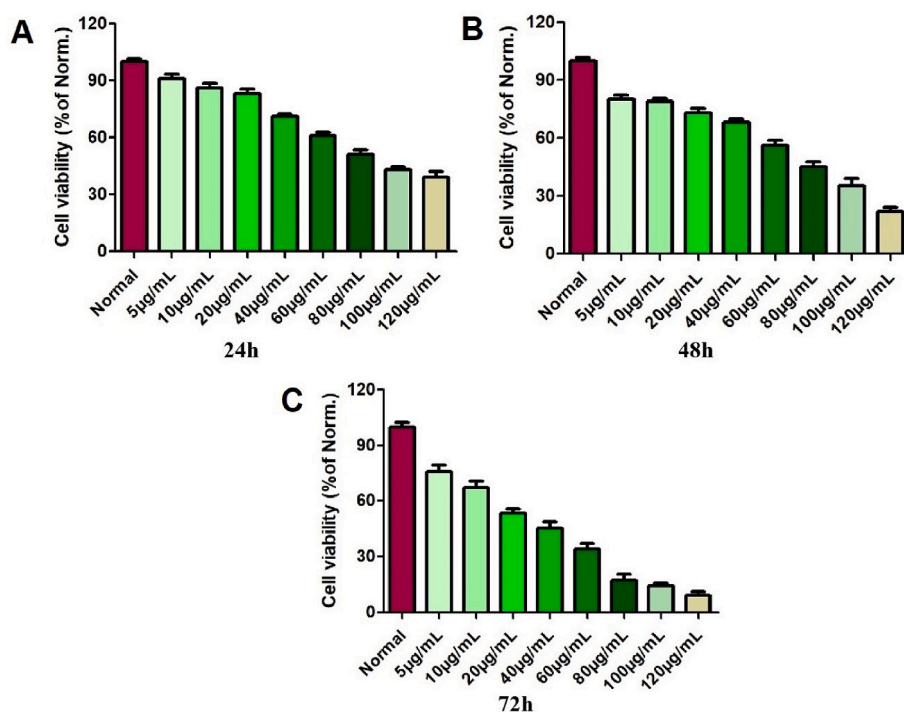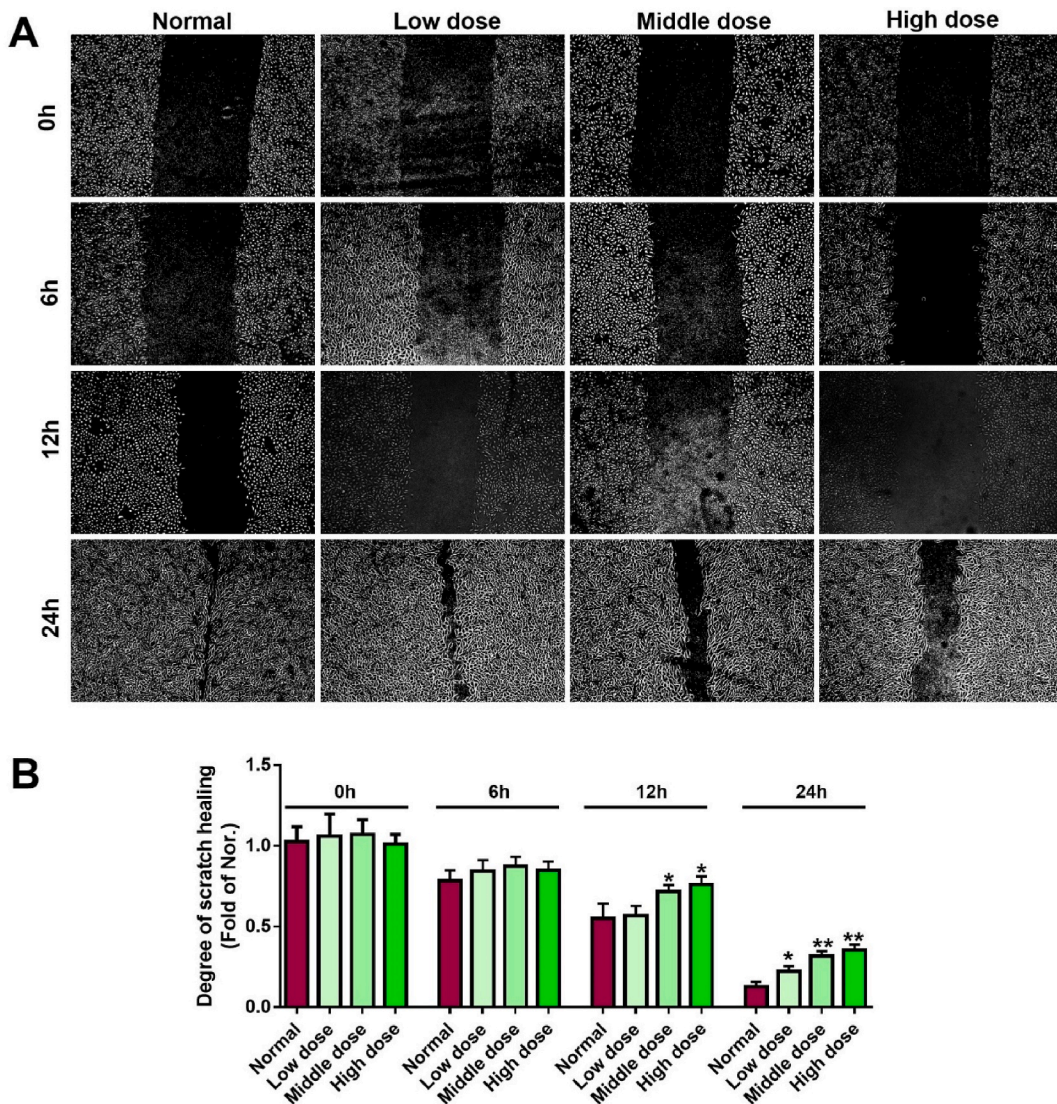

Fig. 5. Effects of the main constituents in HYZ on proliferation of KMH-2 cells in 24 h (**A**), 48 h (**B**), 72 h (**C**).

Fig. 6. HYZ inhibits the migration of KMH-2 cells. (**A**) The represented pictures of wound-healing assays of KMH-2 cells. (**B**) The statistical chart of the would-healing results. **$p < 0.01$ vs. control.

9.10. HYZ can regulate the expression of apoptosis-related proteins in KMH-2 cells

Previous flow cytometry results suggested that HYZ could induce apoptosis of KMH-2 cells. Therefore, we measured the expression of apoptosis-related proteins in the cells. As shown in Fig. 9A–D, HYZ intervention significantly increased the expression of Bad and inhibited its phosphorylation in KMH-2 cells. Similarly, the cleaved-Caspase 3 (C-Caspase 3) levels increased significantly after treatment with different doses of HYZ.

9.11. HYZ inhibited the PI3K-Akt and focal adhesion pathways in KMH-2 cells

The experimental results of network pharmacology suggested that the anti-TC effect of HYZ was related to the PI3K-Akt signaling pathway and focal adhesion pathway. We also found that HYZ could significantly inhibit the migration and invasion of KMH-2 cells and induce apoptosis. To further study the molecular mechanism of the antitumor effect of HYZ, the expression of related proteins in the PI3K-Akt and focal adhesion signaling pathways in KMH 2 cells was determined by WB, and the results are shown in Fig. 9A and E-H. Compared with the control group, phosphorylation of PI3K and AKT was significantly inhibited after HYZ treatment, indicating that HYZ inhibited the activation of the PI3K-Akt pathway in KMH-2 cells. Focal adhesion kinase (FAK) is a multifunctional nonreceptor tyrosine kinase that mediates adhesion between cells and the extracellular matrix, as well as a key link in the focal adhesion pathway. Therefore, we examined the expression of FAK in cells and found that HYZ seemed to have no effect on the expression of proto-FAK, but
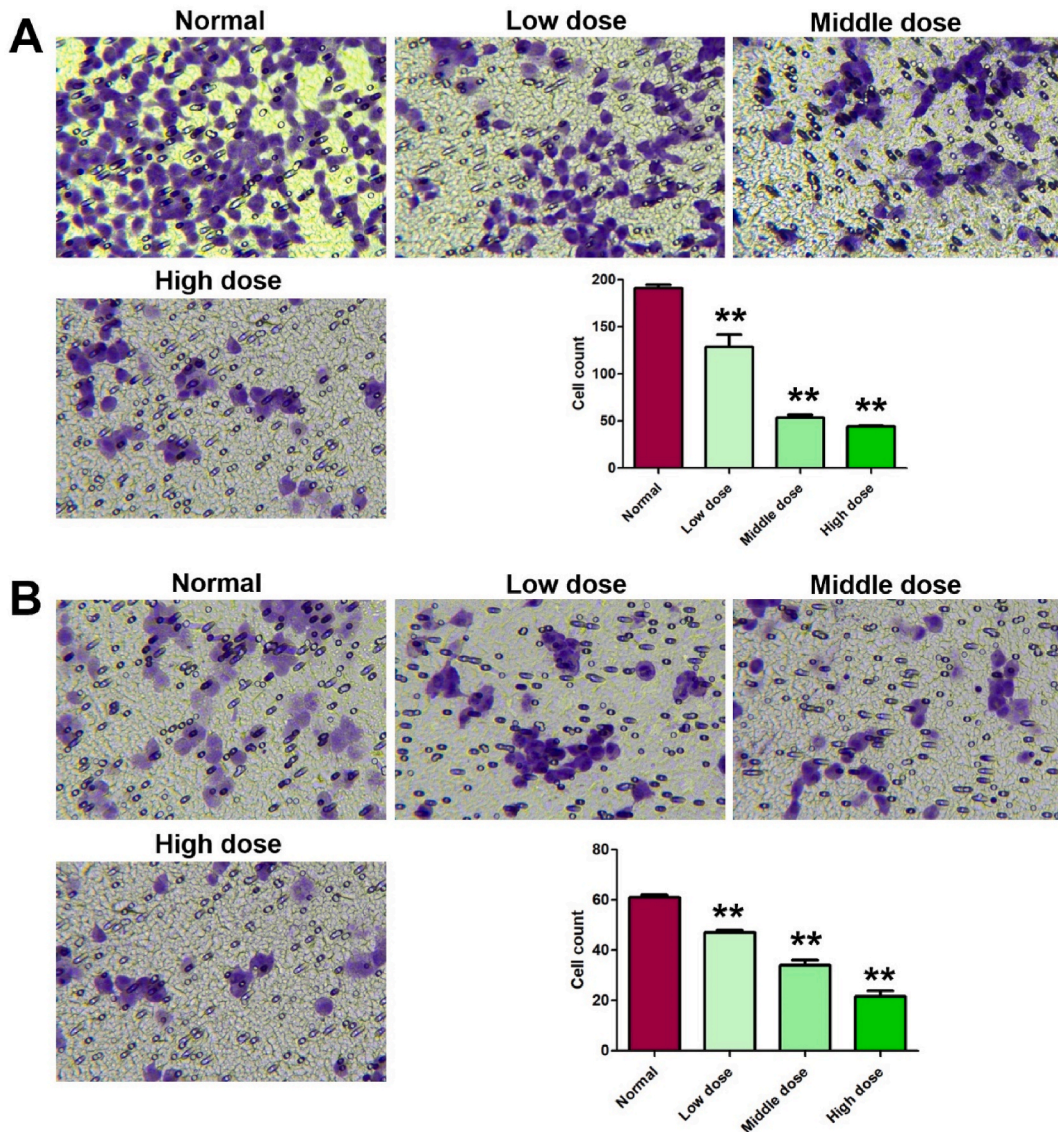
Fig. 7. Effects of HYZ on the migration and invasion ability of KMH-2 cells using Transwell chamber. (**A**) The results of the migration experiment; (**B**) The results of the invasion experiment. **p < 0.01 vs. control.

p-FAK expression in cells decreased significantly after intervention (Fig. 9 A & I–K). Existing studies have shown that E-CAD is a key protein in the metastasis and invasion of many tumor cells, including TC cells. Therefore, we also measured the expression of E-CAD protein in KMH-2 cells after HYZ intervention. As expected, HYZ significantly upregulated the expression of E-CAD protein (Fig. 9 A & I–K).

10. Discussion

TC is currently one of the most common endocrine malignant tumors in the world. The pathogenesis of TC is still unclear, and it is generally believed to be related to the levels of sodium iodine transporters and estrogen. Current clinical treatment methods have difficulty reducing the recurrence rate, while the accompanying treatment side effects and high treatment costs have greatly increased the physical burden and economic burden of patients. Therefore, it is necessary to find more efficient and safer complementary or alternative drugs. With the gradual deepening of scientific research, drugs from natural sources are increasingly sought after by researchers as candidates for antitumor drugs [30]. Tuber *Dioscoreae Bulbiferae* (*Huang Yaozi*, HYZ) is a common medicine used in TCM to treat sore throat, goiter, hematemesis, hemoptysis, and other diseases. It has remarkable clinical effects, low price and few side effects. At the same time, clinical studies have reported that HYZ has a good therapeutic effect on patients with thyroid tumors and TC. In addition, modern studies have also found that HYZ has a good inhibitory effect on the growth of TC cells, but these studies are not
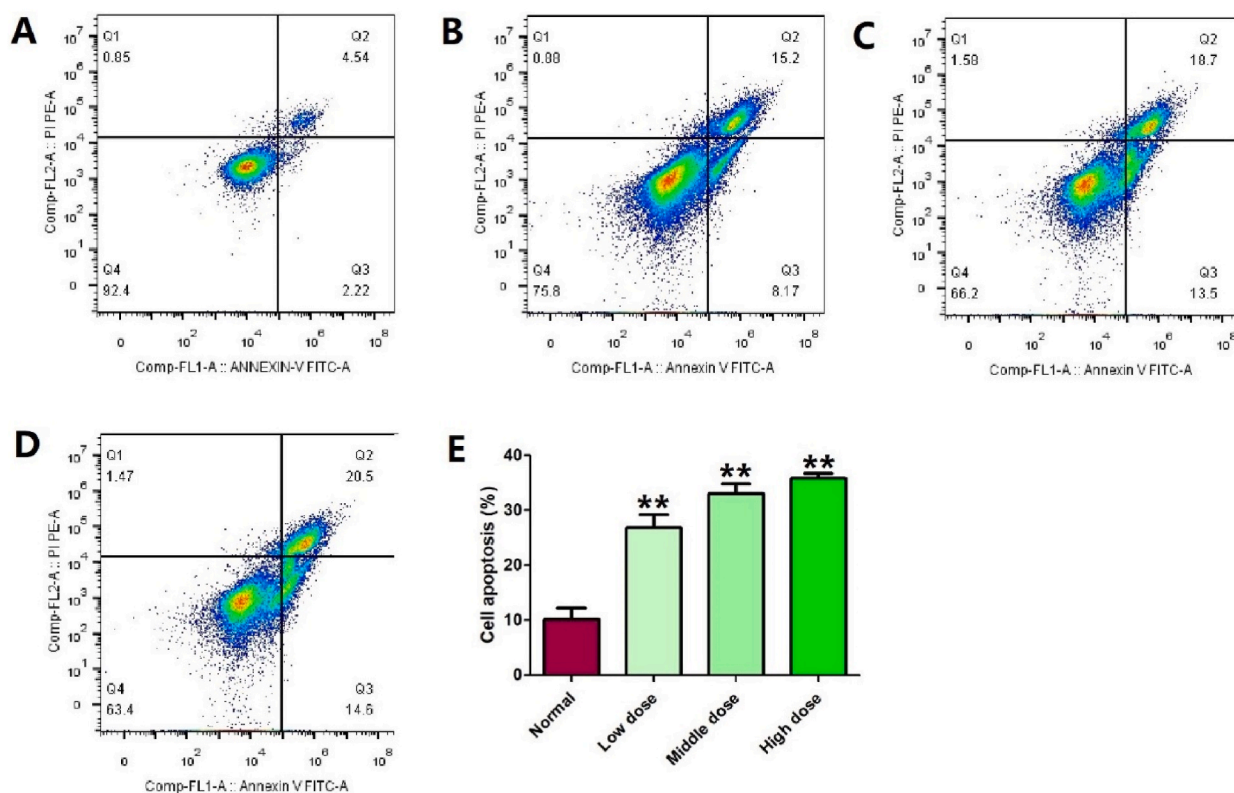
Fig. 8. Apoptotic induction activities of HYZ on KMH-2 cells. Cells were treated with different concentrations of HYZ for 24 h, and the apoptotic effects of HYZ were detected by flow cytometric analysis with Annexin V-FITC and PI staining. (**A**)–(**D**) represents the flow charts of Normal, Low dose, Middle dose, and High dose of HYZ; (**E**) Statistical chart of the flow cytometric analysis. **p < 0.01 vs. control.

in-depth enough to explain the molecular mechanism of HYZ in the treatment of TC. Currently, accumulating herbal medicines are being developed as candidate drugs for treating various difficult miscellaneous diseases, such as cancer [31], neurodegenerative diseases [32], cardiovascular diseases [33], and diabetes mellitus [34].

In this study, network pharmacology combined with bioinformatics methods was used to explore the molecular mechanism by which HYZ exerts its anti-TC effect. The results showed that HYZ could exert anti-TC effects through multicomponent and multitarget methods, and compounds such as C1, C14, C11, C3 and C6 might be the main active components of HYZ against TC. In addition, our results also suggest that the specific mechanism of HYZ against TC may be mainly related to regulating the PI3K-Akt pathway and focal adhesion pathway. To verify the reliability of network pharmacology and bioinformatics experiments, we designed corresponding antitumor experiments in vitro. The CCK8 assay showed that HYZ inhibited the proliferation of KMH-2 cells in a dose-dependent manner. To verify whether the effect of HYZ on cell viability was related to apoptosis induction, the apoptosis of KMH-2 cells after HYZ intervention was determined by flow cytometry. As expected, HYZ could significantly induce apoptosis of KMH-2 cells. Similarly, at the protein level, our study also found that HYZ can inhibit the phosphorylation of Bad and promote the activation of Caspase 3, the executor of apoptosis. It is well known that the PI3K-AKT pathway is closely related to cell growth, proliferation and death [35,36], and network pharmacology results suggest that the antitumor effect of HYZ is related to the regulation of the PI3K-AKT pathway. Therefore, we also determined the expression of PI3K and AKT in KMH-2 cells after HYZ intervention and found that HYZ could significantly inhibit the phosphorylation of PI3K and AKT, confirming that the antitumor effect of HYZ was related to the inhibition of the activation of the PI3K-AKT pathway. In addition, it has been reported that the focal adhesion pathway plays an important role in the migration and invasion of tumor cells [37]. Therefore, we also studied the effect of HYZ on the migration and invasion ability of KMH-2 cells. Fortunately, different doses of HYZ significantly inhibited the migration and invasion of KMH-2 cells. FAK and E-CAD are proteins that play a key role in the metastasis and invasion of many tumor cells, as well as a key link in the focal adhesion pathway [38, 39]. We also found that the expression of p-FAK decreased significantly after HYZ intervention, but the expression of E-CAD protein was significantly upregulated, suggesting that HYZ can inhibit the migration and invasion of thyroid cancer cells by regulating FAK phosphorylation and E-CAD expression in the focal adhesion pathway.

11. Conclusion

In this study, based on network pharmacology and bioinformatics combined with antitumor experiments in vitro, we investigated
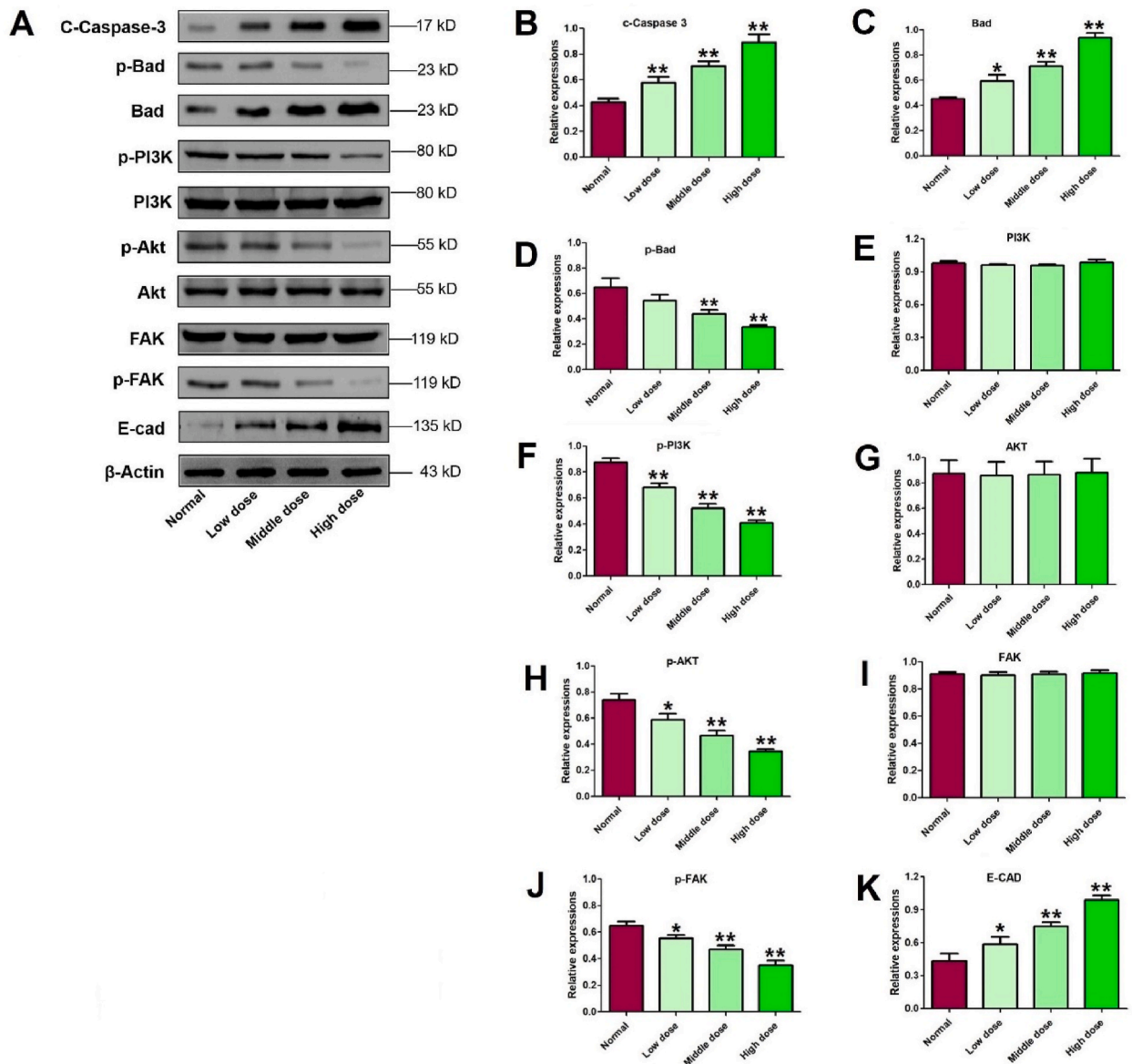
Fig. 9. The Western blot (WB) assay was used to detect the effect of HYZ intervention on protein expression in cells. (**A**) Representative strip images for the WB assay. (D)–(K) is the statistical charts of C-Caspase-3, Bad, p-Bad, PI3K, p-PI3K, Akt, p-Akt, FAK, p-FAK, and E-cad, respectively. C-Caspase-3 means cleaved Caspase-3. *$p < 0.05$, **$p < 0.01$ vs. control.

the inhibitory effect and mechanism of HYZ on the growth, migration, and invasion of KMH-2 human TC cells and found that HYZ could inhibit the growth, migration, and invasion of KMH-2 cells. Importantly, these inhibitory effects are consistent with previous network pharmacology and bioinformatics predictions, that is, regulation of the PI3K-AKT pathway and focal adhesion pathway. The role of prophylactic central neck dissection is still controversial. In more destructive surgery, interventions are affected by more severe complications [40–42]. However, our present study is mainly based on *in silico* and in vitro experiments and is just a "first level study"; thus, in the future, more work should be devoted to evaluating the anti-TC effects of HYZ with a tumor-bearing mouse model and further clinical studies in humans. In addition, more studies should be performed to explore the possible toxicities and real active substances or marker constituents in HYZ.

In conclusion, our study provides a reference for further animal or clinical studies investigating the effectiveness and molecular mechanisms of HYZ against thyroid cancer.

Ethics approval and consent to participate

Not applicable.

Author contribution statement

Ziqi Liu, Lian Zhong, Chao Chen: Conceived and designed the experiments; Performed the experiments; Contributed reagents, materials, analysis tools or data; Wrote the paper. </p>; **Lingyu Wang**: Performed the experiments; Contributed reagents, materials, analysis tools or data. </p>; **Meiyan Li**: Analyzed and interpreted the data. </p>

Funding statement

Data availability statement

Data included in article/supp. material/referenced in article.

Declaration of competing interest

The authors declare that they have no known competing financial interests or personal relationships that could have appeared to influence the work reported in this paper.

Appendix A. Supplementary data

Supplementary data related to this article can be found at https://doi.org/10.1016/j.heliyon.2023.e18886.

References

[1] R.L. Siegel, K.D. Miller, A. Jemal, Cancer statistics, 2017, CA-Cancer, J. Clin. 67 (2017) 7–30.
[2] W. Chen, R. Zheng, P.D. Baade, S. Zhang, H. Zeng, F. Bray, A. Jemal, X.Q. Yu, J. He, Cancer statistics in China, 2015, CA cancer, J. Clin. 66 (2016) 115.
[3] W.Q. Chen, R.S. Zheng, S.W. Zhang, Analysis of incidence and death of malignant tumors in China in 2012, Chin. Cancer 25 (2016) 1–8.
[4] R.L. Siegel, K.D. Miller, A. Jemal, Cancer statistics, 2020, CA A Cancer J. Clin. 70 (2020) 7–30.
[5] H.R. Harach, G.A. Ceballos, Thyroid cancer, thyroiditis and dietary iodine: a review based on the Salta, Argentina model, Endocr. Pathol. 19 (2008) 209–220.
[6] J.Y. Zhu, X.T. Li, C.F. Xie, P3.02c-012 apatinib, a new small molecular VEGFR2 inhibitor, suppresses the activity of lung cancer stem cells, J. Thoracic. Oncol. 12 (2017) S1279.
[7] I.G. Papanikolaou, Oncoplastic breast-conserving surgery in breast cancer treatment Systematic review of the literature, Ann. Ital. Chir. 87 (2016) 199–208.
[8] V.C. Ezeocha, J.S. Nwogha, A.N. Ohuoba, Evaluation of poultry manure application rates on the nutrient composition of *Dioscorea bulbifera* (Aerial yam), Niger. Food. J. 32 (2014) 92–96.
[9] B. Dutta, Food and medicinal values of certain species of *Dioscorea* with special reference to Assam, J. Pharmacogn. Phytochem. 3 (2015) 15–18.
[10] S. Ghosh, V.S. Parlihar, P. More, D.D. Dhavale, B.A. Chopade, Phytochemsitry and therapeutic potential of medicinal plant: *Dioscorea bulbifera*, Med. Chem. 5 (2015) 160–172.
[11] M.R. Bhandari, J. Kawabata, Organic acid, phenolic content and antioxidant activity of wild yam (Dioscorea spp.), Tube. Nepal, Food Chem. 88 (2004) 163–168.
[12] F.L. Song, R.Y. Gan, Y. Zhang, Q. Xiao, L. Kuang, H.B. Li, Total phenolic contents and antioxidant capacities of selected Chinese medicinal plants, Int. J. Mol. Sci. 11 (2010) 2362–2372.
[13] V. Kuete, R. Betrandteponno, A.T. Mbaveng, L.A. Tapondjou, J.J.M. Meyer, L. Barboni, N. Lall, Antibacterial activities of the extracts, fractions and compounds from *Dioscorea bulbifera*, BMC Complement. Altern. Med. 12 (2012) 228.
[14] H. Gao, M. Kuroyanagi, L. Wu, N. Kawahara, T. Yasuno, Y. Nakamura, Antitumor-promoting constituents from *Dioscorea bulbifera* L. in JB6 mouse epidermal cells, Biol. Pharm. Bull. 25 (2002) 1241–1243.
[15] J.M. Wang, L.L. Ji, C.J. Branford-White, Z.Y. Wang, K.K. Shen, H. Liu, Z.T. Wang, Antitumor activity of *Dioscorea bulbifera* L. rhizome in vivo, Fitoterapia 83 (2012) 388–394.
[16] S. Ghosh, M. Ahire, S. Patil, A. Jabgunde, M.B. Dusane, B.N. Joshi, K. Pardesi, S. Jachak, D.D. Dhavale, B.A. Chopade, Antidiabetic activity of gnidia glauca and *Dioscorea bulbifera*: potent amylase and glucosidase inhibitors, evid. Based. Complement, Alternat. Med. 2012 (2012), 929051.
[17] M. Mbiantcha, A. Kamanyi, R.B. Teponno, A.L. Tapondjou, P. Watcho, T.B. Nguelefack, Analgesic and anti-Inflammatory properties of extracts from the bulbils of *Dioscorea bulbifera* L. var sativa (Dioscoreaceae) in mice and Rats, Evid. Based. Complement. Alternat. Med. 2011 (2011), 912935.
[18] G. Song, Analysis on the treatment of thyroid tumor, Inner. Mongolia. TCM. 26 (2007) 18–19.
[19] W.Y. Zhang, B. Zhang, Treatment of 64 cases of thyroid tumor with chaixia xiaoying decoction, Chin. J. Nat. Med. 5 (2003) 93.
[20] J.X. Zhao, D. Deng, X.Q. Wang, Textual research on the names of TCM diseases related to thyroid diseases, J. Shaanxi. Univ. TCM. 28 (2005) 2.
[21] Y. Lin, K. Ma, Q.L. Li, A case study of Professor Ma Ke in the diagnosis and treatment of thyroid cancer, Inner. Mongolia, TCM 36 (2017) 95–96.
[22] Y.Y. Zhao, X.J. Chu, H.Y. Pu, Effect of huangyaozi on survivin gene and protein expression of thyroid cancer cell line sw579, Chin. Sci. Technol. TCM. 1 (2012) 320–321.
[23] J. Ru, P. Li, J. Wang, W. Zhou, B. Li, C. Huang, P. Li, Z. Guo, W. Tao, Y. Yang, X. Xu, Y. Li, Y. Wang, L. Yang, TCMSP: a database of systems pharmacology for drug discovery from herbal medicines, J. Cheminform. 6 (2014) 13.
[24] L. Guo, D.Z. Xia, Y.J. Luo, Discussion on the mechanism of tufuling in the treatment of gout based on network pharmacology, Chin. Herb. Med. 50 (2019) 1413–1418.
[25] X. Liu, S. Ouyang, B. Yu, Y. Liu, K. Huang, J. Gong, S. Zheng, Z. Li, H. Li, H. Jiang, PharmMapper server: a web server for potential drug target identification using pharmacophore mapping approach, Nucleic Acids Res. 38 (2010) W609–W614.

[26] X. Wang, C. Pan, J. Gong, X. Liu, H. Li, Enhancing the enrichment of pharmacophore-based target prediction for the polypharmacological profiles of drugs, J. Chem. Inf. Model. 56 (2016) 1175–1183.

[27] X. Wang, Y. Shen, S. Wang, S. Li, W. Zhang, X. Liu, L. Lai, J. Pei, H. Li, PharmMapper 2017 update: a web server for potential drug target identification with a comprehensive target pharmacophore database, Nucleic Acids Res. 45 (2017) W356–W360.

[28] A. Daina, O. Michielin, V. Zoete, SwissTargetPrediction: updated data and new features for efficient prediction of protein targets of small molecules, Nucleic Acids Res. 47 (2019) W357–W364.

[29] D. Gfeller, O. Michielin, V. Zoete, Shaping the interaction landscape of bioactive molecules, Bioinformatics 29 (2013) 3073–3079.

[30] Q. Zhang, H. Duan, R. Li, J. Sun, J. Liu, W. Peng, C. Wu, Y. Gao, Inducing apoptosis and suppressing inflammatory reactions in synovial fibroblasts are two important ways for *guizhi-shaoyao-zhimu* decoction against rheumatoid arthritis, J. Inflamm. Res. 14 (2021) 217–236.

[31] D. Tewari, P. Patni, A. Bishayee, A. N Sah, A. Bishayee, Natural products targeting the PI3K-Akt-mTOR signaling pathway in cancer: a novel therapeutic strategy, Semin. Cancer Biol. 80 (2022) 1–17.

[32] W. Peng, Y. Chen, S. Tumilty, L. Liu, L. Luo, H. Yin, Y. Xie, Paeoniflorin is a promising natural monomer for neurodegenerative diseases via modulation of Ca^{2+} and ROS homeostasis, Curr. Opin. Pharmacol. 62 (2022) 97–102.

[33] Q. Zhang, J. Liu, H.X. Duan, R. Li, W. Peng, C. Wu, Activation of Nrf2/HO-1 signaling: an important molecular mechanism of herbal medicine in the treatment of atherosclerosis via the protection of vascular endothelial cells from oxidative stress, J. Adv. Res. 34 (2021) 43–63.

[34] V. Lakshmanakumar, G. Arthi, J. Rathinam, V. Harishanbuselvan, D. Sivaraman, Molecular docking analysis to validate the efficacy of traditional siddha polyherbal Formulation Aavarai Bhavanai Chooranam (ABC) against enzyme alpha-glucosidase for type II diabetes mellitus, TMR. Integr. Med. 7 (2023), e23001.

[35] M. Luo, Y. Zheng, S. Tang, L. Gu, Y. Zhu, R. Ying, Y. Liu, J. Ma, R. Guo, P. Gao, C. Zhang, Radical oxygen species: an important breakthrough point for botanical drugs to regulate oxidative stress and treat the disorder of glycolipid metabolism, Front. Pharmacol. 14 (2023), 1166178.

[36] H. Duan, Q. Zhang, J. Liu, R. Li, D. Wang, W. Peng, C. Wu, Suppression of apoptosis in vascular endothelial cell, the promising way for natural medicines to treat atherosclerosis, Pharmacol. Res. 168 (2021), 105599.

[37] S. Wu, M. Chen, J. Huang, F. Zhang, Z. Lv, Y. Jia, Y. Cui, L. Sun, Y. Wang, Y. Tang, K.R. Verhoeft, Y. Li, Y. Qin, X. Lin, X. Guan, K. Lam, ORAI2 promotes gastric cancer tumorigenicity and metastasis through PI3K/Akt signaling and MAPK-dependent focal adhesion disassembly, Cancer Res. 81 (2021) 986–1000.

[38] F.J. Sulzmaier, C. Jean, D.D. Schlaepfer, FAK in cancer: mechanistic findings and clinical applications, Nat. Rev. Cancer 14 (2014) 598–610.

[39] D. Wang, L. Su, D. Huang, H. Zhang, D.M. Shin, Z.G. Chen, Downregulation of E-Cadherin enhances proliferation of head and neck cancer through transcriptional regulation of EGFR, Mol. Cancer 10 (2011) 116.

[40] C. Gambardella, R. Patrone, F.D. Capua, C. Offi, C. Mauriello, G. Clarizia, C. Andretta, A. Polistena, A. Sanguinetti, P. Calò, G. Docimo, N. Avenia, G. Conzo, The role of prophylactic central compartment lymph node dissection in elderly patients with differentiated thyroid cancer: a multicentric study, BMC Surg. 18 (2019) 110.

[41] G. Conzo, G. Docimo, R. Ruggiero, S. Napolitano, A. Palazzo, C. Gambardella, C. Mauriello, E. Tartaglia, F. Cavallo, L. Santini, Surgical treatment of papillary thyroid carcinoma without lymph nodal involvement, G. Chir. 33 (2012) 339–342.

[42] G. Conzo, P.G. Calò, C. Gambardella, E. Tartaglia, C. Mauriello, C.D. Pietra, F. Medas, R.S. Cruz, F. Podda, L. Santini, G. Troncone, Controversies in the surgical management of thyroid follicular neoplasms. Retrospective analysis of 721 patients, Int. J. Surg. 12 (2014) S29–S34.